AN APPROACH TO OPTIMIZE REFERENCE GROUND CONTROL REQUIREMENTS FOR ESTIMATING LIDAR/IMU BORESIGHT MISALIGNMENT

A. Pothou[a,*], C. Toth[c], S. Karamitsos[b], A. Georgopoulos[a]

[a] Laboratory of Photogrammetry - (apothou, drag)@central.ntua.gr
[b] Laboratory of Higher Geodesy - karamits@central.ntua.gr
School of Rural & Surveying Engineering, National Technical University of Athens, Greece

[c]Center for Mapping, The Ohio State University, 1216 Kinnear Road, Columbus, OH 43212 USA – toth@cfm.ohio-state.edu

WG I/2, XXI Congress ISPRS, 2008 China

KEY WORDS: Boresight misalignment, GPS, IMU, Direct Georeferencing, MMS, LiDAR, QA/QC

ABSTRACT:

LiDAR systems are complex multi-sensory systems and include at least three main sensors: GPS, IMU navigation sensors, and the laser-scanning device. High-performance integrated GPS/IMU systems provide the navigation solution for the LiDAR data acquisition platform, and therefore, the proper calibration, including individual and inter-sensor calibration, is a must to achieve the highest accuracy of the output data. Specifically regarding the boresight misalignment, the spatial relationship between the IMU body frame and the LiDAR body frame is of high importance as it could be the largest source of systematic errors in airborne MMS, and thus must be determined before the system can be effectively utilized. In this research, the feasibility of using urban areas for boresight misalignment is investigated. In particular, the impact of the building shape, size, distribution, etc. on the performance of the boresight misalignment process, is of interest. In this study, photogrammetrically restituted buildings were used as the reference surfaces, called 'building-positions' or 'reference-positions'. The influence of the number of 'building-positions' and their distribution on the boresight's misalignment parameter estimation is investigated and evaluated through QA/QC statistical tests.

1. INTRODUCTION

LiDAR (Light Detection And Ranging, also known as Airborne Laser Scanning – ALS) is a highly automated and still rapidly evolving technology, with excellent vertical accuracy of point measurements. LiDAR has many benefits, and is quickly becoming the prime technology for large-scale acquisition of elevation data due to its capability to directly measure 3D coordinates of a huge number of points. LiDAR systems are complex multi-sensory systems including: GPS (Global Positioning System), and IMU (Inertial Measurement Unit, also known as INS Inertial Navigation System) navigation sensors, and the laser-scanning device. Most of the new systems also include a medium format digital camera to provide conventional image coverage of the surveyed area. A variety of highly specialized systems based on modern imaging sensors, such as CCD cameras, LiDAR, and hyper/multi-spectral scanners, have been developed in the last decade. LiDAR is considered as a basic component of airborne Mobile Mapping Systems (MMS) (for details see Bossler and Toth, 1995; Schwarz *et al.*, 1993; El-Sheimy *et al.*, 1995). The proper calibration of this MMS, including individual and inter-sensor calibration, is a must to achieve the highest accuracy of the output data. Particularly regarding the boresight misalignment, the spatial relationship between the IMU body frame and the LiDAR body frame is of high importance, as it could be the largest source of systematic errors in airborne MMS, and thus, must be determined before the system can be effectively utilized (Burman, 2000). In most installations, the lever arms between LiDAR/GPS/IMU sensors can be determined separately by independent means, with good accuracy. In sharp contrast, the determination of the boresight angles is only possible in-flight once the GPS/IMU derived orientation becomes sufficiently accurate (Skaloud and Lichti, 2006).

Despite several years of progress, the boresight estimation between the LiDAR and IMU sensors is still heavily researched. Baltsavias (1999) presents an overview of basic relations and error formulas concerning airborne laser scanning. Also a large number of publications report the existence of systematic errors (Schenk, 2001; Filin, 2001). The solutions for dealing with and eliminating the effect of systematic boresight misalignment errors can be categorized into two groups. Techniques in the first group are based on the introduction of a correction transformation of the laser points to minimize the difference between the corresponding LiDAR points and the ground truth; for instance, Kilian *et al.* (1996), Pothou *et al.* (2007), use surface patches while Csanyi and Toth, (2007) investigate the achievable LiDAR data accuracy improvement using LiDAR-specific ground control targets. This technique is frequently called data driven. In contrast, the other group attempts to rigorously model the system to recover the systematic errors (Burman, 2000) and treats the discrepancies between overlapping strips, including navigation and sensor calibration errors, as orientation errors.

Since the ground surfaces are not always known, or at the required accuracy level, preference has been given to techniques which do not require a priori knowledge of the surface (Toth and Csanyi, 2001; Toth *et al.*, 2002). This alternative solution is independent from ground control, and can determine the boresight misalignment angles using overlapping LiDAR strips, flown in different directions.

Not long ago, another rigorous class of calibration procedures started to emerge (Filin, 2003; Friess, 2006; Skaloud and Lichti, 2006; Scaloud and Schaer, 2007). These types of approaches model all systematic errors directly in the measurement domain and condition groups of points to reside on a common surface of known form.

The earlier methods, related to LiDAR strip adjustment, also addressed the effects of systematic errors in the registration

* Corresponding author

(which was based on DEM matching) of overlapping point clouds. For extended literature review about co-registration, see in Pothou *et al.,* 2006a; Pothou *et al.,* 2006b.
Currently the most common method of calibrating a LiDAR sensor is also the least rigorous: profiles of overlapping strips are compared and an experienced operator manually adjusts the misalignment angles until the strips appear to visually fit. Although practical, this approach is time consuming and labor intensive and the results do not immediately provide any statistical measure on the quality of the calibration (Morin and El-Sheimy, 2002). Furthermore, the existing methods often cannot reliably recover all three of the angular mounting parameters. The undetermined parameter(s) propagate into the subsequently captured data, therefore compromising the accuracy of any derived product. Thus, much research effort is still devoted to improve these processes. Most of the adopted approaches are usually based on either physical boundaries or cross-sections (Schenk, 2001) or DTM/DSM gradients (Burman, 2000), mimicking the photogrammetric calibration approach via signalized or intensity-deduced targets points. The drawbacks of these methods is the lack (or simplification) of assurance measures, correlation with the unknown terrain shape or limits imposed by laser pointing accuracy and uncertainty due to beam-width. Habib *et al.* (2007), proposed a LiDAR system self-calibration using planar patches derived from photogrammetric data. Not only is the mathematical model for the LiDAR system calibration by using control planar patches presented but also the optimal configuration for flight conditions and the distribution of planar patches, to avoid possible correlations have also been analysed.

Pothou *et al.* (2007), introduced a novel prototype algorithm for observing, and subsequently determining the boresight misalignment of LiDAR/IMU, using two different surfaces (point datasets). This algorithm minimizes the distances between points of the target surface and surface patches (TINs) of the reference surface, along the corresponding surface normals (based on Schenk *et al.,* 2000). The technique can be applied to various data combinations, such as matching LiDAR strips or comparing LiDAR data to photogrammetrically derived surfaces. Object of simple shape similar to man-made structures, such as buildings, have been chosen and constructed to perform the surface matching. The processing algorithm includes additional testing of the validity, accuracy, and precision of various statistical tests (QA/QC - Quality Assurance/Quality Control) for outlier detection in positioning and attitude data.
In this research, the feasibility of using urban areas for boresight misalignment is investigated. Buildings are of particular interest; in other words, what the impact of the building shape, size, distribution, etc. is on the performance of the boresight misalignment process. Photogrammetrically restituted buildings were used as reference surfaces called 'building-positions' or 'reference-positions'. The influence of the number and distribution of the necessary 'building-positions' on boresight's misalignment parameter estimation is evaluated. Experiments with various number of 'building-positions' in regular as well as random distribution are presented, analyzed and evaluated through QA/QC statistical tests. The optimum number and distribution of 'building-positions' have been determined and proposed.
In Section 2, a short review of the status of multi-sensor calibration and boresight misalignment of LiDAR/IMU is provided. Section 3 outlines the mathematical model of the algorithm for the boresight misalignment and presents the statistical analysis of the QA/QC techniques supported by the LiDAR/IMU boresight misalignment calculation. In Section 4, the dataset used for testing is described. The experimental results, as well as their statistical analysis and their effects on LiDAR points, are described in Section 5. Section 6 concludes the research.

2. MULTI SENSOR CALIBRATION - BORESIGHT MISALIGNMENT

The IMU frame is usually considered as the local reference system of the MMS system, and thus, the navigation solution is computed within this frame. The spatial relationship between the laser scanner and the IMU is defined by the offset and rotation between the two systems. To obtain the local object coordinates of a LiDAR point, the laser range vector has to be reduced to the IMU system by applying the offsets and rotations between the two systems, which provides the coordinates of the LiDAR point in the IMU system. The GPS/IMU based navigation provides the orientation of the IMU frame, including position and attitude, and thus, the mapping frame coordinates can be subsequently derived. In our discussion, the determination of the boresight offset (b_x, b_y, b_z) and the boresight matrix (rotations ω, φ, κ) between the IMU and the laser frame (provided that sufficient ground control is available) is addressed.
Any discrepancy in boresight values results in a misfit between the LiDAR points and the ground surface, and thus, the calculated coordinates of the LiDAR points are not correct (Toth, 2002). Ideally, the calibration parameters should stay constant for subsequent missions. The description of the effects of the different boresight misalignment angles is omitted here; for details see (Baltsavias, 1999). For a detailed description of multisensor calibration – boresight misalignment, see Toth and Csanyi, 2001; Toth, 2002; Pothou *et al.,* 2007.

3. MATHEMATICAL MODEL OF THE ALGORITHM

Two datasets, called point clouds, P (x_{pi}, y_{pi}, z_{pi}) (p_i= 1,…, n) and Q (x_{qi}, y_{qi}, z_{qi}) (q_i= 1,…, m), which describe the same object are captured by different technologies and they must be transformed into a common system. Assuming that these datasets are connected by a 6-parameter 3D transformation, the three offset and three rotation parameters can be estimated, minimizing the distance between a point of Q dataset and a TIN surface patch of P surface, which is described by points of P dataset (Equation 1). In Figure 1, point q_i (x_{qi}, y_{qi}, z_{qi}) of Q point cloud, has to be transformed to the closest surface patch of the control surface P, defined by 3 points (p_m, p_k, p_l), through its projection q_i' (x_{qi}', y_{qi}', z_{qi}') onto the surface patch. In Pothou *et al.,* 2006b, details for the algorithm were presented (it is called algorithm B). Also in Pothou *et al.,* 2007, analysis and performance of this algorithm, for the boresight parameters estimation was proposed.
In Equation 1, **R** (ω, φ, κ) is the orthogonal rotation matrix, defined in Equation 2, while b_x, b_y, b_z are the elements of the offset vector.

$$\begin{bmatrix} x_p \\ y_p \\ z_p \end{bmatrix} = \mathbf{R} \cdot \begin{bmatrix} x_q \\ y_q \\ z_q \end{bmatrix} + \begin{bmatrix} b_x \\ b_y \\ b_z \end{bmatrix} \quad (1)$$

$$\mathbf{R} = \begin{bmatrix} \cos\varphi\cos\kappa & \cos\omega\sin\kappa + \sin\omega\sin\varphi\cos\kappa & \sin\omega\sin\kappa - \cos\omega\sin\varphi\cos\kappa \\ -\cos\varphi\sin\kappa & \cos\omega\cos\kappa - \sin\omega\sin\varphi\sin\kappa & \sin\omega\cos\kappa + \cos\omega\sin\varphi\sin\kappa \\ \sin\varphi & -\sin\omega\cos\varphi & \cos\omega\cos\varphi \end{bmatrix} \quad (2)$$

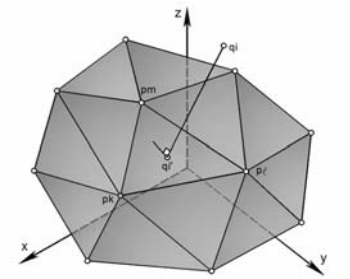

Figure 1: Transformation between q_i points and control surface P

The parameters of the plane's equation (which passes from the 3 known points (p_m, p_k, p_ℓ)), are given by the derivatives in Equation 3.

$$A=\begin{vmatrix} y_{pm} & z_{pm} & 1 \\ y_{pk} & z_{pk} & 1 \\ y_{p\ell} & z_{p\ell} & 1 \end{vmatrix} \quad B=\begin{vmatrix} x_{pm} & z_{pm} & 1 \\ x_{pk} & z_{pk} & 1 \\ x_{p\ell} & z_{p\ell} & 1 \end{vmatrix}$$
$$C=\begin{vmatrix} x_{pm} & y_{pm} & 1 \\ x_{pk} & y_{pk} & 1 \\ x_{p\ell} & y_{p\ell} & 1 \end{vmatrix} \quad D=\begin{vmatrix} x_{pm} & y_{pm} & z_{pm} \\ x_{pk} & y_{pk} & z_{pk} \\ x_{p\ell} & y_{p\ell} & z_{p\ell} \end{vmatrix} \tag{3}$$

Based on Equation 3, the coordinates of q_i' (x_{qi}', y_{qi}', z_{qi}'), which correspond to projection of point q_i (x_{qi}, y_{qi}, z_{qi}) on the plane (p_m, p_k, p_ℓ), can be calculated as described by Pothou *et al.,* 2006a. In order to perform the transformation between the two datasets, the transformed coordinates of point q_i have to be used in the calculation of x_{qi}', y_{qi}', z_{qi}'. So, after the input of Equation 1 to the equations for the calculation of x_{qi}', y_{qi}', z_{qi}', (based on that the difference of each point of dataset Q and its projection on the P surface should be equal to zero), the Equation 5 is derived in which the **T** and **L** are the matrices of Equation 4 that depend on the plane's parameters of Equation 3.

$$\mathbf{T}=\begin{bmatrix} 1-\frac{A^2}{A^2+B^2+C^2} & \frac{BA}{A^2+B^2+C^2} & -\frac{CA}{A^2+B^2+C^2} \\ \frac{AB}{A^2+B^2+C^2} & 1-\frac{B^2}{A^2+B^2+C^2} & \frac{CB}{A^2+B^2+C^2} \\ -\frac{AC}{A^2+B^2+C^2} & \frac{BC}{A^2+B^2+C^2} & 1-\frac{C^2}{A^2+B^2+C^2} \end{bmatrix} \quad \mathbf{L}=\begin{bmatrix} \frac{AD}{A^2+B^2+C^2} \\ -\frac{BD}{A^2+B^2+C^2} \\ \frac{CD}{A^2+B^2+C^2} \end{bmatrix} \tag{4}$$

$$(\mathbf{T}-\mathbf{I})\cdot\left(\mathbf{R}\cdot\begin{bmatrix} x_{qi} \\ y_{qi} \\ z_{qi} \end{bmatrix}+\begin{bmatrix} b_x \\ b_y \\ b_z \end{bmatrix}\right)+\mathbf{L}=\mathbf{0} \tag{5}$$

Equation 5 is the observation equation for each point Q, therefore it is the base for producing the system of Equation 6 which is provided through the Taylor expansion linearization for the parameters (b_x, b_y, b_z, ω, φ, κ). After having performed least squares estimation the solution of Equation 6 and the best estimation of the vector $\hat{\mathbf{x}}$, is provided by Equation 7.

$$\mathbf{A}\delta\mathbf{x}=\boldsymbol{\delta}\ell+\mathbf{v} \tag{6}$$

$$\hat{\mathbf{x}}=\mathbf{x}^{o}+\left(\mathbf{A}^{T}\mathbf{W}\mathbf{A}\right)^{-1}\mathbf{A}^{T}\mathbf{W}\boldsymbol{\delta}\ell \tag{7}$$

In Equations 6 and 7, **A** is the design matrix, **W** is a diagonal weight matrix of the observations, $\mathbf{x}^o$ is the vector of the approximated parameters, $\boldsymbol{\delta}\ell=\ell-\ell^o$ is the second part of the observation equation in which $\ell=\mathbf{0}$ and ℓ^o is the result of Equation 5 using $\mathbf{x}^o$, and finally **v** is the residual vector.

Applying this algorithm for each building, which has been photogrammetrically restituted (P surface), the best estimation of the six parameters (offsets and rotations) is provided. In this process, photogrammetric restitution and LiDAR strips which both are available, the algorithm takes place, setting the proximity between each LiDAR point and each TIN from the building as a choice criterion.
The corresponding covariance matrix of $\hat{\mathbf{x}}$ and the a' posteriori variance of unit weight $\hat{\sigma}_o^2$ are calculated as following where r is the degree of freedom.

$$\hat{\mathbf{V}}_{\hat{x}}=\hat{\sigma}_o^2\left(\mathbf{A}^{T}\mathbf{W}\mathbf{A}\right)^{-1} \tag{8}$$

$$\hat{\sigma}_o^2=\frac{\mathbf{v}^{T}\mathbf{W}\mathbf{v}}{r} \tag{9}$$

Applying the algorithm for each building, in combination with available LiDAR strips, a number of independent estimations of transformation parameters are provided. The redundancy of estimations provides the ability of chosen desirable number and type of estimations i,…, j, in order to provide a unique estimation of the parameters. This can be achieved if a set of chosen solutions is assumed as observations creating a new linear system of observation equations such as Equation 10.
The confrontation of the solution of this system is the same as Equations 6 and 7. The matrix of observations ℓ includes the best estimations of each solution i, …, j which have been chosen from the total of the solutions.

$$\mathbf{A}\hat{\mathbf{x}}=\ell+\mathbf{v} \tag{10}$$

The solution of Equation 10 by Equation 11 is same as that of Equation 7, for the case of linear equations.

$$\hat{\mathbf{x}}=\left(\mathbf{A}^{T}\mathbf{W}\mathbf{A}\right)^{-1}\mathbf{A}^{T}\mathbf{W}\ell \tag{11}$$

In Equation 11, the weight matrix **W** is equal to $\mathbf{W}=\sigma_o^2\mathbf{V}_\ell^{-1}$ where $\mathbf{V}_\ell$ includes the a' posteriori partial covariance matrices of each best estimation, of each solution.
It should be mentioned that due to the fact that partial solutions are non-correlated, the best estimation of Equation 11 is equivalent to the corresponding estimation. This can be calculated from the simultaneous solution of buildings and LiDAR points, which have taken place in the initial solutions of the system 10 through Equations 6 and 7. The a' posteriori standard deviation of unit weight $\hat{\sigma}_o^2$ with the corresponding covariance matrices of the parameters and the observations are calculated based on Equations 8, 9 and 13.

$$\mathbf{V}_\ell=\begin{bmatrix} \hat{\mathbf{V}}_{\hat{x}_i} & \cdots & \mathbf{0} \\ \vdots & \ddots & \vdots \\ \mathbf{0} & \cdots & \hat{\mathbf{V}}_{\hat{x}_j} \end{bmatrix} \tag{12}$$

$$\hat{\mathbf{V}}_{\hat{\ell}}=\hat{\sigma}_o^2\mathbf{A}\left(\mathbf{A}^{T}\mathbf{W}\mathbf{A}\right)^{-1}\mathbf{A}^{T} \tag{13}$$

The statistical valuation of the adjustment's results concerns not only the assumptions, which have been made (initial hypothesis

H_o) related to mathematical and statistical model of adjustment, but also the reliability of the observations.

The general check of this hypothesis H_o is achieved by using the ratio $\hat{\sigma}_o^2/\sigma_o^2$ in combination with the χ^2 distribution, with r degree of freedom.

The hypothesis H_o, according to the reliability of the observations, is checked based on the ratio $\hat{v}_i/\hat{\sigma}_{\hat{v}_i}$ of each observation i by using the normal distribution z for a level meaningfulness α=0.001.

The data snooping procedure led to the conclusion that approximately 4%-5% of the observations include outliers. The above results are in agreement with what have been proven in Pothou *et al.,* 2007.

4. DATA DESCRIPTION

After implementing the proposed method, it was first tested on the simulated data for boresight misalignment estimation (Pothou et al., 2007). Next a new dataset, provided by ODOT (Ohio Department of Transportation) and CFM (The Center for Mapping, OSU) was used for intensive testing. In London, Madison County, Ohio, LiDAR point clouds and direct digital aerial images were collected in several missions over an urban test area. The city includes mainly residential houses and a few bigger buildings (such as warehouses and factories).

The 55 mm focal length, DSS digital camera, with 9μm pixel size, was laboratory calibrated prior to the test flights. The test area was simultaneously surveyed by an Optech ALTM 30/70 LiDAR system of the Ohio Department of Transportation. At FOV of 40°, 50 Hz scanner frequency and 70 kHz pulse rate, the point density was about 5-8 points/m^2. A set of 16 images with adequate coverage of the region, which contained survey control points, was identified. The flight plan consisted of two parallel strips and two perpendicular strips. Therefore, the data contain 4 LiDAR strips (point cloud) and a block of 4 aerial images strips over the same area, each containing 4 images (Figure 2). For both sensors, an integrated GPS/IMU system provided the georeferencing. Traditional aerotriangulation was performed on aerial images using GCPs measured by geodetic means (0.1m stdv) producing the EO (Exterior Orientation). The bundle adjustment resulted in positioning accuracies (EO parameters) averaging 0.08, 0.08, and 0.10 meters in X, Y, and Z, respectively. The orientation accuracies average 10, 10, and 9 arcsecs in ω, φ, κ, respectively.

In the central part of the survey (also called "test field") 24 buildings, mainly medium sized, have been selected and photogrammetrically restituted (point dataset). These buildings (called 'buildings-positions') are located in the overlapping area. In Figure 2, an image mosaic, the selected buildings and LiDAR strips are illustrated. These buildings are assumed as the reference dataset. The area which is occupied by the selected group of buildings is about 300,000 m^2 with a perimeter of 2250 m.

As it has been mentioned, that proposed method assumes that the reference dataset is derived by photogrammetric means (surface P) and the target dataset consists of the corresponding LiDAR points (surface Q) captured over the same overlapped area. It should be mentioned that the reference dataset can be derived by any other source such as by terrestrial laserscanning. But in this research, they were aerial photos of interest.

Figure 2: Highlighted buildings distributed in the area and LiDAR strips' orientation

5. EXPERIMENTS AND RESULTS

The first part of the algorithm is an enhanced version of Pothou *et al.,* 2007 method which calculates the boresight misalignment parameters and their standard deviation for each strip over each individual building. In this individual solution a data snooping procedure eliminates outliers before estimating the boresight parameters (Equation 7). The second part of the algorithm calculates the total solution (Equation 11) where combinations of buildings and strips are involved (with their individual weights).

In the first part, the results for each strip over each individual building point out to some learning (Figure 3). Redundancy (observations) can enhance the results namely buildings with many observations (points) give better results. Buildings with very small or big stdv, in their individual solutions, give extremely different weights from the mean stdv to the solution. They should be avoided from the total solution setting up a threshold for big and small buildings, so only the medium size buildings remain in the solution. The following thresholds were used: (LiDAR 500-2000 points) and (TINs 500-1500). Although the algorithm is capable of detecting these types of errors (σ_x, σ_y, σ_z), some buildings with errors have been located. Possible errors can originate due to the photogrammetric restitution (e.g. building 12). Through data snooping procedure LiDAR points, 4-5% outliers are removed and the parameters are stabilized. It is illustrated in Figures 5, 6 e.g. for angle omega. The boresight offset components cannot be detected accurately in this type of data due to high correlation of parameters and noise. Thus in case of a bigger offset, it could be detected (σ_x, σ_y, $\sigma_z > b_x$, b_y, b_z).

In the second part, the results of the total solutions were analyzed, indicating that the algorithm can absorb the existence of at least 15% 'problematic-out of threshold' buildings. This should be considered as a restriction of this algorithm. Through many tests with differently distributed buildings, it can be concluded that positions similar to the Gruber positions, widely used in photogrammetry, (6-8 buildings) are the optimum (Figure 4). It can be noticed that the shape of buildings don't affect the results. This type of distribution of the buildings has been actually confirmed in LiDAR boresight misalignment solution (Csanyi and Toth, 2007). Combinations of strips are necessary: at least, 2 strips flying in opposite directions are

needed to recover the signs of the parameters. Also a 3rd strip, in a crossing direction, is preferred for enhancing the incompleteness of the parallel strips. This cross strip could decrease the effects of possible systematic errors which could arise from many sources e.g. different flying height between strips.

6. CONCLUSIONS

The feasibility of using urban areas for boresight misalignment has been investigated. The influence of the number and distribution of the necessary 'building-positions' on boresight's misalignment parameter estimation is evaluated. Experiments with various number and distribution of 'building-positions' are presented, analyzed and evaluated through QA/QC statistical tests.

Under operational circumstances, the real accurate values of the boresight misalignment are never accurately known and could only be estimated. Furthermore, boresight misalignment parameters could change over a relatively short time period. Therefore, having a mechanism to almost continuously check it is a valuable tool. In other words, the detection of possible changes in the values (in the remaining boresight misalignment) through a QA/QC validation process, can assure a sustained product's quality. These algorithms can be considered as a good and fast tool for estimating parameters and detecting any changes.

It is noticeable that this algorithm in not restricted by detailed restitution, as only the main skeleton of a building is needed. This is different from some other algorithms where, for instance, the availability of roof planes is a prerequisite. In this algorithm buildings should include points within the threshold range, and at least 2 strips flying in opposite directions are necessary; obviously a good distribution of the buildings is the necessity to reach an optimum.

7. REFERENCES

Baltsavias, E.P., (1999). Airborne laser scanning: basic relations and formulas. *ISPRS Journal of Photogrammetry & Remote Sensing* 54, pp.199-214.

Bossler, J. D., and Toth, C., (1995). Accuracies Obtained by the GPSVan^{TM}. *GIS/LIS*, Vol. 1, pp. 70-77.

Burman, H., (2000). Adjustment of Laser Scanner Data for Correction of Orientation Errors. *IAPRS*, Vol. XXXIII, Part B3, pp.125-132.

Csanyi, N., and Toth, C., (2007). Improvement of LiDAR Data Accuracy Using LiDAR-Specific Ground Targets. *PE&RS,* Volume 73, Number 4.

El-Sheimy, N., Schwarz, K. P., Gravel, M., (1995). Mobile 3-D Positioning Using GPS/INS/Video Cameras. *Mobile Mapping Symposium, OSU Center for Mapping*, pp. 236-249.

Filin, S., (2001). Recovery of Systematic Biases in Laser Altimeters Using Natural Surfaces. *IAPRS,* Vol. XXXIV, Part 3/W4, pp. 85-91.

Filin, S., (2003). Analysis and implementation of a laser strip adjustment model. *IAPRS,* 34(3/W13), pp.65-70.

Friess, P., (2006). Toward a rigorous methodology for airborne laser mapping. *International Calibration and Orientation Workshop EuroCOW* 2006.

Habib, A., Bang, K.I., Shin S., Mitishita E., (2007). LiDAR system self-calibration using planar patches from photogrammetric data. MMT'07*, 'The 5th International Symposium on Mobile Mapping Technology'*.

Kilian, J., Haala, N., Englich, M., (1996). Capture and Evaluation of Airborne Laser Scanner Data. *IAPRS*, Vol. XXXI, Part B3, pp. 383-388.

Morin, K., and El-Sheimy, N., (2002). Post-mission adjustment of airborne laser scanning data. *Proceedings XXII FIG International Congress*, Washington DC, USA, CD ROM.

Pothou A., Karamitsos S., Georgopoulos A., and Kotsis I., (2006a). Performance evaluation for aerial images and airborne Laser Altimerty dara registration procedures. *ASPRS,* Nevada.

Pothou A., Karamitsos S., Georgopoulos A., and Kotsis I., (2006b). Assessment and comparison of registration algorithms between aerial images and laser point clouds. *ISPRS*, Com. 1, *Symposium:'From sensor to imagery'* WGI/2, Part A, France.

Pothou A., Toth C., Karamitsos S., and Georgopoulos A., (2007). On using QA/QC techniques for LiDAR/IMU boresight misalignment. MMT'07*, 'The 5th International Symposium on Mobile Mapping Technology'*.

Schwarz, K. P., Chapman, M., Cannon, M. E., and Gong, P., (1993). An Integrated INS/GPS Approach to the Georeferencing of Remotely Sensed Data. *PE&RS*, Vol. 59/11, pp. 1667-1674.

Skaloud, J., and Lichti D., (2006). Rigorous approach to boresight self-calibration in airborne laser scanning. *ISPRS, Journal of Photogrammetry & Remote Sensing* 61, pp. 47-59.

Skaloud, J., and Schaer, P., (2007). Towards automated LiDAR Boresight self-calibration. MMT'07*, 'The 5th International Symposium on Mobile Mapping Technology'*.

Schenk, T., Krupnik A., and Postolov Y., (2000). Registration of airborne laser data to surfaces generated by Photogrammetric means. *IAPRS*, 32(3/W14) pp.95-99.

Schenk, T., (2001). Modeling and Analyzing Systematic Errors in Airborne Laser Scanners. *Technical Notes in Photogrammetry,* vol. 19, The Ohio State University, Columbus, USA.

Toth, C., and Csanyi, N., (2001). Automating the LiDAR Boresight Misalignment. *ISPRS WGII/2 Workshop on 3-D Mapping from InSAR and LiDAR*, Banff, Canada, CD ROM.

Toth, C., Csanyi, N., and Grejner Brzezinska, D. A., (2002). Automating the Calibration of Airborne Multisensor Imaging Systems. *ACSM/ASPRS/FIG Congress and Annual Conference*, Washington, DC, CD ROM.

Toth, C., (2002). Calibrating Airborne LiDAR Systems, ISPRS Commission II Symposium on Integrated Systems for Spatial Data Production. Custodian and Decision Support, *IAPRS*, Vol. XXXIV, part 2, pp.475-480.

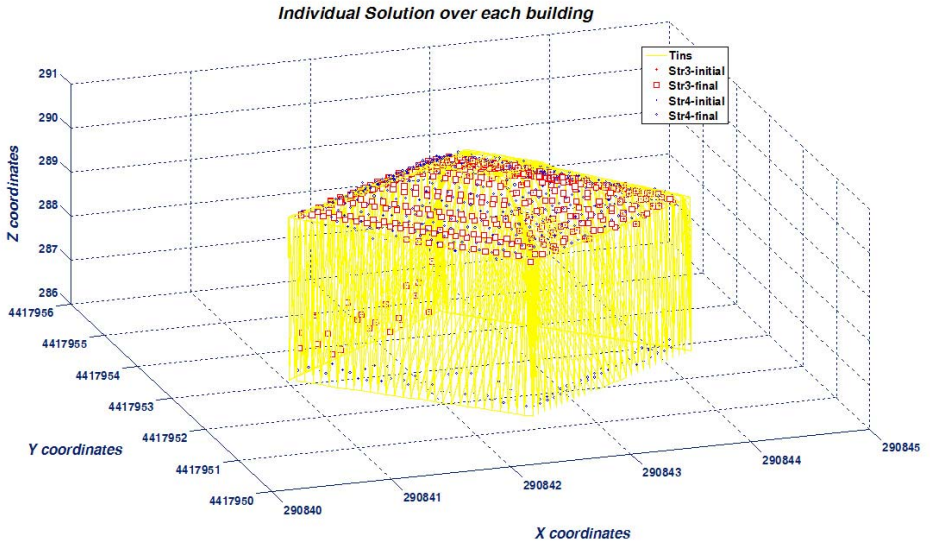

Figure 3: LiDAR strips over each individual building (e.g. building 18) for the calculation of boresight parameters

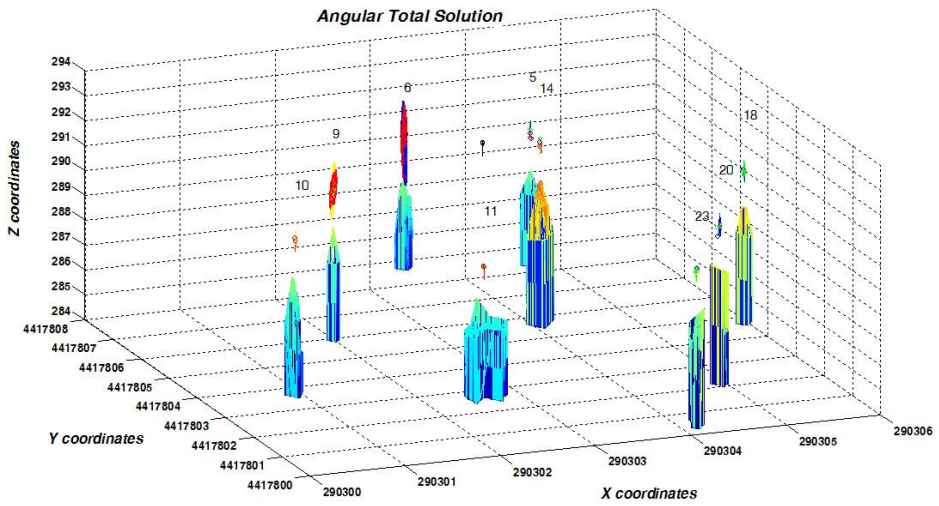

Figure 4: Angular total solution combining buildings for the calculation of boresight parameters

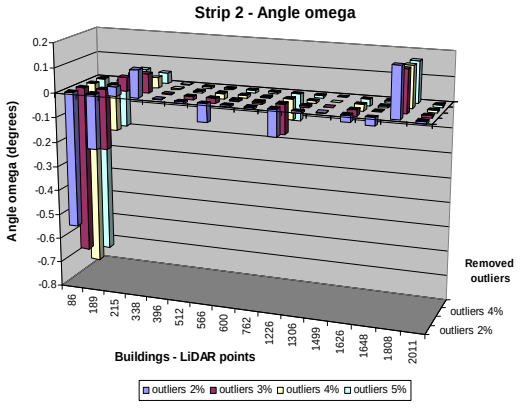

Figure 5: Angle omega per number of LiDAR points

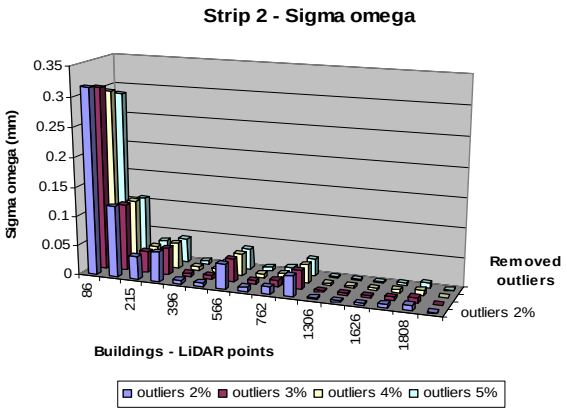

Figure 6: Sigma omega per number of LiDAR points